Applied Physics A (2019) 125:17
https://doi.org/10.1007/s00339-018-2306-x

Applied Physics A
Materials Science & Processing

Refractive index changes and optical absorption involving 1*s*–1*p* excitonic transitions in quantum dot under pressure and temperature effects

N. Aghoutane[1] · M. El-Yadri[1] · A. El Aouami[1] · E. Feddi[1] · F. Dujardin[2] · M. El Haouari[1,3] · C. A. Duque[4] · Chuong V. Nguyen[5] · Huynh V. Phuc[6]

Received: 6 September 2018 / Accepted: 3 December 2018 / Published online: 11 December 2018

Abstract
The pressure and temperature effects on the optical responses involving the $1s-1p$ intersubband transition of an exciton in a spherical quantum dot are investigated. Calculations are performed in the framework of the effective mass approximation and the energies are obtained by using a Ritz variational method. Our approach is based on the Hylleraas formalism were the correlations between the electron and hole are taken into account. Temperature, pressure and the size effects on the linear and third nonlinear optical properties are analyzed. Our results show that the temperature and pressure provide important effects on linear and nonlinear parts of the absorption coefficient (AC) and the relative refractive index change (RI) associated to the $1s-1p$ transition. We found that by increasing the temperature and pressure the AC and RI curves shift to lower and higher energies respectively. Calculations show also that the dot size affects considerably the AC and RI and their corresponding amplitude.

1 Introduction

Due to their wide range applications in different domains (biology, electronic, photonic, energy storage among others) [1–4], the semiconductors nanomaterials continue to receive increased and special attraction. Their original properties are attributed to their nano sizes and therefore to the confinement effects. Indeed, the reduction of the size leads to quantization of electronic states, enhancement of orbitals overlap and strengthening of the binding energies of donors, excitons or excitonic complexes. All these properties induces important changes in optical properties of the nanomaterials [5, 6] which open the way to the realization of new optoelectronic devices. A particular interest has been focused on the nonlinear optical properties. Thus, numerous investigations have treated the nonlinear optical effects associated to the intersubband transitions in various situations: with and without external perturbations such as magnetic field, electric field, pressure and temperature [7–10]. It has been demonstrated that the nonlinear optical responses are sensitive to the asymmetry of the confining potential and to the size and the shape of the structure. Among the most significant results we can cite Yildrim et al. [11] who have demonstrated that the nonlinear part of absorption coefficient (AC) of GaAs quantum dots (QDs) is affected by both the geometrical asymmetry and the effect of electric field. Kostic and Stojanovic have treated the nonlinear absorption spectra for intersubband transitions of CdSe/ZnS spherical quantum dots described by a spherical potential. They have determined the fundamental energy state of electrons and first excited states (s, p, and d) using the effective mass approximation. Their results show that the nonlinear optical

✉ F. Dujardin
francis.dujardin@univ-lorraine.fr

[1] Laboratoire de Matière Condensée et Sciences Interdisciplinaires (LaMCScI), Group of Optoelectronic of Semiconductors and Nanomaterials, ENSET, Mohammed V University, Rabat, Morocco

[2] Université de Lorraine, LCP-A2MC, 57000 Metz, France

[3] Centre Régional des Métiers de l'Education et de Formation (CRMEF), Tangier, Morocco

[4] Grupo de Materia Condensada-UdeA, Instituto de Física, Facultad de Ciencias Exactas y Naturales, Universidad de Antioquia UdeA, Calle 70 No. 52-21, Medellín, Colombia

[5] Department of Materials Science and Engineering, Le Quy Don Technical University, Ha Noi 100000, Viet Nam

[6] Division of Theoretical Physics, Dong Thap University, Cao Lãnh, Dong Thap 870000, Viet Nam

properties associated with $1s$–$1p$, $1p$–$1d$, and $1p$–$2s$ transitions are greatly dependent on the QD size and structure [12].

The nonlinear optical coefficients and refractive index changes related to the presence of donor centre has been investigated in the parabolic confinement, by using Potential Morphing Method [13] and by the matrix diagonalization approach [14]. These studies have shown that the optical responses are strongly influenced by three factors: confinement strength, incident optical intensity and presence of impurities. In addition, the orientation of the incident light polarization constitute an important factor influencing the nonlinear susceptibility [15]. In relation with pressure, theoretical studies have shown that for all types of confinement the absorption coefficient resonant-peaks are blue shifted and their intensities increase with increasing pressure and the nonlinear properties are very sensitive to the ionized donor position in the structure [16]. More recently, the hydrostatic pressure induced band diagram of an InGaAsN/GaAs spherical quantum dot system was theoretically calculated using an expanded form of standard 8 band k.p Hamiltonian [17]. The optical gain for a GaAs spherical quantum dot laser was also studied under pressure and temperature by Owji et al. [18].

It is worth mentioning that the majority of these studies have neglected the effect of electron hole correlations on the nonlinear optical properties. Indeed, in the QDs, the 3D confinement leads to an enhancement of the oscillator strength associated to the electron–hole recombination. Therefore, the Coulomb interactions lead to a significant change of the linear and nonlinear optical properties [19]. Thus, taking into account the excitonic effects is unavoidable mainly in the confined systems.

Unfortunately, analyzing the existing literature, we noticed that the majority of the studies were limited to the nonlinear optical properties related to the transitions between the non-interacting and interacting (via a coulombic potential) electron–hole pair but very few theoretical studies are devoted to the investigations of the nonlinear optical properties associated to the excitonic transitions. One of the first attempts is that made by Hanamura [20] who has shown that the third nonlinear optical response is enhanced in QDs with larger exciton binding energy and small effective Bohr radius such as in I–VII and II–VI semiconductors. In the framework of effective mass approximation and by using a perturbation method, Lu et al. [21] have investigated the optical properties of exciton under pressure, temperature and electric field. The authors highlighted that the excitonic effects can not be neglected. Let's emphasize that their calculations have shown that the effect of the temperature is underestimated and their conclusion concerning the pressure and confinement effects is questionable (we will return to this point in the discussion of our results).

In order to show the contribution of the excitonic states transitions on the nonlinear optical properties, we investigate the linear and nonlinear optical properties associated to $1s$–$1p$ excitonic transition in single quantum dots under the pressure and temperature effects. Thus, we attempt to discover the behavior of linear and nonlinear absorption coefficients and the change of the refractive indexes involving the first allowed excitonic transition. We also analyze the effect of temperature and hydrostatic pressure. Calculations are performed in the framework of the effective mass approximation and the energies are obtained by using a variational method and by choosing an appropriate wave function taking into account the different inter-particle correlations for $1s$ and $1p$ states. This paper is organized as follows: in Sect. 2 we present our detailed theoretical analysis to determine the eigenstates and the optical properties for the $1s-1p$ intersubband transition. Our numerical results and discussions are reported in Sect. 3.

2 Background theory

In the framework of the effective mass approximation and under the effect of external hydrostatic pressure P and temperature T, an interacting electron–hole (exciton) in a GaAs spherical QD surrounded by a material with large band gap is described by the Hamiltonian:

$$H_X = -\frac{\hbar^2}{2\,m_{\mathrm{e}}^*(P,T)}\Delta_{\mathrm{e}} - \frac{\hbar^2}{2\,m_{\mathrm{h}}^*(P,T)}\Delta_{\mathrm{h}} - \frac{e^2}{\varepsilon(P,T)r_{\mathrm{eh}}} + V_w^{\mathrm{e}} + V_w^{\mathrm{h}}, \tag{1}$$

with $r_{\mathrm{eh}} = \left|\overrightarrow{r_{\mathrm{e}}} - \overrightarrow{r_{\mathrm{h}}}\right|$, $\vec{r}_{\mathrm{e}}$ and $\overrightarrow{r_{\mathrm{h}}}$ are the electron and hole coordinates. $\varepsilon(P,T)$ and $m_i^*(P,T)$ are respectively the pressure and temperature dependent dielectric constant and effective masses of particle i ($i = \mathrm{e}, \mathrm{h}$). The pressure and temperature dependences follow the relations [22, 23]:

$$\begin{cases} m_{\mathrm{e}}^*(P,T) = m_0\left[1 + 7.51\left(\frac{2}{E_{\mathrm{g}}(P,T)} + \frac{1}{E_{\mathrm{g}}(P,T)+\Delta_0}\right)\right]^{-1} \\ m_{\mathrm{h}}^*(P,T) = m_0\left(0.09 - 0.2\times10^{-3}P - 3.55\times10^{-5}T\right) \end{cases}, \tag{2}$$

where m_0 is the free electron mass and Δ_0 is the spin orbit splitting. $E_{\mathrm{g}}(P,T)$ is the pressure dependent GaAs band gap at the centre Γ of the Brillouin zone, it can be expressed in eV by the relation [22, 24] :

$$E_{\mathrm{g}}(P,T) = 1.519 - \frac{5.4\times10^{-4}T^2}{T+204} + 0.01261\,P + 3.77\times10^{-5}P^2, \tag{3}$$

and

$$\varepsilon(P,T)=\begin{cases}12.7\exp(-1.67\times10^{-3}P)\exp(9.4\times10^{-5}(T-75.6)) & \text{for } 0\le T\le 200\,\text{K}\\ 13.18\exp(-1.73\times10^{-3}P)\exp(20.4\times10^{-5}(T-300)) & \text{for } T>200\,\text{K}\end{cases}. \tag{4}$$

In this work, we treat the case where the QDs are supposed immersed in a wide band dielectric medium such as curable resin or another polymer with a very large gap. Because of this large band offsets between the QD and the external medium, the electronic density is more localized inside the dot. This justify the choice of an infinite confinement potential:

$$V_w^i=\begin{cases}0 & r_i(P,T)\le R(P,T)\\ \infty & r_i(P,T)>R(P,T)\end{cases} i=(\text{e},\text{h}). \tag{5}$$

It has been proven that in nanomaterials, all physical parameters are assigned by the strain effects [25]. The sizes with and without pressure are always related to the elastic constants by assuming that the dot radius follows the behavior:

$$R(P)=R(0)\left[1-(S_{11}+2S_{12})P\right]^{1/3}, \tag{6}$$

where $R(0)$ is the radius without pressure ($P=0$), S_{11} and S_{12} are the compliance parameters which are related to the elastic constants C_{11} and C_{12} by the relations [26–28]:

$$S_{11}=\frac{C_{11}+C_{12}}{(C_{11}-C_{12})(C_{11}+2C_{12})} \quad \text{and}$$
$$S_{12}=\frac{C_{12}}{(C_{11}-C_{12})(C_{11}+2C_{12})}. \tag{7}$$

By using the excitonic units $a_X=\varepsilon\hbar^2/\text{e}^2\mu$ for length and $R_X=\hbar^2/2\mu a_X^2$ for energy, where $\mu=(\frac{1}{m_\text{e}^*}+\frac{1}{m_\text{h}^*})^{-1}$ is the exciton reduced mass, the Hamiltonian in Eq. (1) becomes:

$$H_X=-\frac{1}{(1+\sigma)}\left[\frac{m_\text{e}^*}{m_\text{e}^*(P,T)}\right]\Delta_\text{e} -\frac{\sigma}{(1+\sigma)}\left[\frac{m_\text{h}^*}{m_\text{h}^*(P,T)}\right]\Delta_\text{h}-\frac{2\varepsilon}{\varepsilon(P,T)r_\text{eh}}, \tag{8}$$

where $\sigma=\frac{m_\text{e}^*}{m_\text{h}^*}$ is the electron to hole mass ratio.

Strictly speaking, the exciton can be treated as a two body system whose the parametrization requires six degrees of freedom. However, because of the invariance by rotation of all states about the z-axis, only five coordinates are needed. In our previous studies [29–31], we have shown that the coordinates $(r_\text{e}, r_\text{h}, r_\text{eh}, z_\text{e}, z_\text{h})$ used by Atanasoff [32] are well appropriate for this type of calculations. In these systems, the Laplacian Δ_e can be transformed as:

$$\Delta_\text{e}=-\frac{\partial^2}{\partial r_\text{e}^2}-\frac{\partial^2}{\partial r_\text{eh}^2}-\left(\frac{r_\text{e}^2-r_\text{h}^2+r_\text{eh}^2}{r_\text{e}r_\text{eh}}\right)\frac{\partial^2}{\partial r_\text{e}\partial r_\text{eh}}-\frac{2}{r_\text{e}}\frac{\partial}{\partial r_\text{e}} -\frac{2}{r_\text{eh}}\frac{\partial}{\partial r_\text{eh}}-\frac{2z_\text{e}}{r_\text{e}}\frac{\partial^2}{\partial z_\text{e}\partial r_\text{e}}-2\left(\frac{z_\text{e}-z_\text{h}}{r_\text{eh}}\right)\frac{\partial^2}{\partial z_\text{e}\partial r_\text{eh}}-\frac{\partial^2}{\partial z_\text{e}^2}, \tag{9}$$

while Δ_h is obtained by interchanging the subscripts e and h. The energy E_X and the corresponding envelope wave function Ψ_X are solutions for the Schrödinger equation $H_X\Psi_X=E_X\Psi_X$. This equation cannot be solved analytically, so the eigenvalues must be determined numerically using, for example, a variational method. The energy is obtained by the minimization of the mean value of H:

$$E_X=\min\frac{\langle\Psi_i|H|\Psi_i\rangle}{\langle\Psi_i|\Psi_i\rangle},\quad i=1s,\ 1p. \tag{10}$$

The trial wave functions are chosen as:

$$\Psi_{(n,l,m)}=R_n(r_\text{e},r_\text{h},r_\text{eh},z_\text{e},z_\text{h})Y_l^m(\theta,\varphi), \tag{11}$$

where $Y_l^m(\theta,\varphi)$ are the spherical harmonics, $R_n(r_\text{e},r_\text{h},r_\text{eh},z_\text{e},z_\text{h})$ are the radial wave functions which can be expressed in terms of Bessel functions [33], l is the orbital quantum number, m is the magnetic quantum number, and n is the quantum number which corresponds to the number of solutions of the dispersion equation (when l is fixed).

In this study we focus on the excitonic transition between the fundamental $1s$ ($n=1$, $l=0$, $m=0$) and the first excited $1p$ ($n=1$, $l=1$, $m=0$) states as follows:

$$\Psi_{1s}=N_0 j_0(r_\text{e})j_0(r_\text{h})\,Y_0^0(\theta_\text{e},\varphi_\text{e})\,Y_0^0(\theta_\text{h},\varphi_\text{h})\,\text{e}^{-\alpha r_\text{eh}}, \tag{12}$$

$$\Psi_{1p}=N_1 j_1(r_\text{e})j_1(r_\text{h})\,Y_1^0(\theta_\text{e},\varphi_\text{e})\,Y_1^0(\theta_\text{h},\varphi_\text{h})\,r_\text{eh}\,\text{e}^{-\beta r_\text{eh}}, \tag{13}$$

where j_0 and j_1 are the zero order and the first order spherical Bessel functions respectively. N_0 and N_1 are the normalization constants. The state energies are obtained by minimizing the mean value (10) by respect to the variational parameters α and β. In order to calculate the different integrals we use the elementary volume in Hylleraas coordinates:

$$\text{d}v=\frac{8\pi r_\text{e}r_\text{h}r_\text{eh}\text{d}r_\text{e}\text{d}r_\text{h}\text{d}r_\text{eh}\text{d}z_\text{e}\text{d}z_\text{h}}{Q}, \tag{14}$$

where the denominator Q is given by:

$$Q = \sqrt{4\,(r_e^2 - z_e^2)(r_h^2 - z_h^2) - (r_e^2 + r_h^2 - r_{eh}^2 - 2\,z_e\,z_h)^2}. \quad (15)$$

The integrations over z_e and z_h were performed by generalization of Atanasoff integrals [32] and done in domains $-r_e \le z_e \le r_e$ and $Z_1 \le z_h \le Z_2$ where Z_1 and Z_2 are the roots of the Q expression.

In order to study the optical responses related to this kind of elementary transitions, we introduce the oscillator strength P_{fi} associated with the electronic dipole-allowed transition, which constitutes a measurable magnitude in photoluminescence spectra. Its expression is given by the Fermi golden rule:

$$P_{fi} = \frac{2m_e^*}{\hbar^2}|M_{fi}|^2 E_{fi}, \quad (16)$$

where $E_{fi} = E_f - E_i$ denotes the energy transition between the final $1p$ and initial $1s$ states, $M_{fi} = e\,\langle\Psi_i|\vec{r_e} - \vec{r_h}|\Psi_f\rangle = e\,\langle\Psi_i|r_{eh}|\Psi_f\rangle$ is the electric dipole moment of the transition between the states i and f with the selection rule on the quantum number l ($\Delta l = \pm 1$).

Based on the compact density matrix approach, the total refractive index change can be written as [34–36]:

$$\frac{\Delta n(\omega)}{n_r} = \frac{\Delta^{(1)} n(\omega)}{n_r} + \frac{\Delta^{(3)} n(\omega)}{n_r}. \quad (17)$$

The first and second expressions in the right member are respectively the linear and nonlinear terms of refractive index (RI), they are given by:

$$\frac{\Delta^{(1)} n(\omega)}{n_r} = \frac{1}{2\varepsilon_0 n_r^2}\frac{\sigma_1 |M_{fi}|^2 (E_{fi} - \hbar\omega)}{(E_{fi} - \hbar\omega)^2 + (\hbar\Gamma_{fi})^2}, \quad (18)$$

and

$$\frac{\Delta^{(3)} n(\omega)}{n_r} = -\frac{\mu_1 c I \sigma_1 |M_{fi}|^4}{\varepsilon_0 n_r^3}\frac{(E_{fi} - \hbar\omega)}{\left[(E_{fi} - \hbar\omega)^2 + (\hbar\Gamma_{fi})^2\right]^2} \left[1 - \frac{(M_{ff} - M_{ii})^2}{4|M_{fi}|^2(E_{fi}^2 + (\hbar\Gamma_{fi})^2)}\left\{E_{fi}(E_{fi} - \hbar\omega) - (\hbar\Gamma_{fi})^2 - (\hbar\Gamma_{fi})^2\frac{(2E_{fi} - \hbar\omega)}{(E_{fi} - \hbar\omega)}\right\}\right]. \quad (19)$$

In the previous expressions, c stands for the velocity of light in vacuum, σ_1 is the electron density related to the occupied volume by the relation $\sigma_1 = \frac{n}{V(P)}$, $V(P)$ is the pressure dependent sphere volume, I is the intensity of the incident electromagnetic field, μ_1 is the permeability of the system, n_r is the relative refractive index of the QD, ε_0 is the dielectric constant of the vacuum, $\hbar\omega$ is the incident photon energy

Table 1 Physical parameters of GaAs and light properties [37]

$m_e^* = 0.067\,m_0$	$m_h^* = 0.079\,m_0$
$\sigma_1 = 0.848$	$\varepsilon = 13.18$
$E_g = 1.607$ eV	$\Delta_0 = 0.341$ eV
$n = 3.2$	$\sigma = 3 \times 10^{22}$ m^{-3}
$\Gamma_{fi} = 0.2$ ps^{-1}	$I = 200$ MW/m^2
$S_{11} = 1.16 \times 10^{-2}$ GPa^{-1}	$a_X = 19.24$ nm
$S_{12} = -3.7 \times 10^{-3}$ GPa^{-1}	$R_X = 2.84$ meV

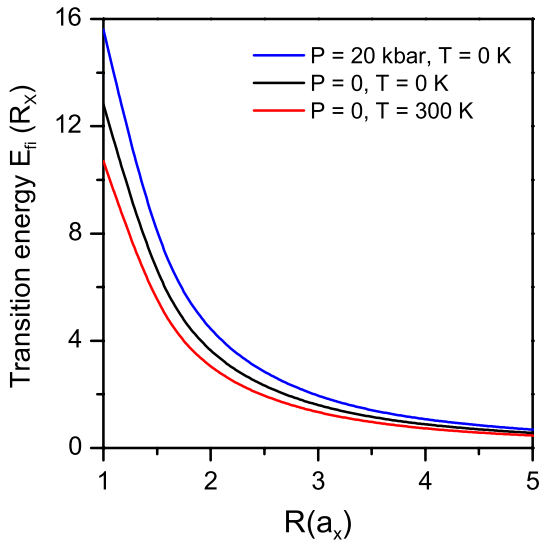

Fig. 1 Energy difference between ground and first excited states as a function of the dot radius, for ($P = 0$, $T = 0$ K) and ($P = 20$ kbar, $T = 0$ K)

and finally, the non-diagonal matrix element Γ_{fi} is defined as the inverse of the relaxation time τ_{fi} and known as relaxation rate of final and initial states. The same formalism allows to obtain the total absorption coefficients (AC):

$$\alpha(\omega, I) = \alpha^{(1)}(\omega) + \alpha^{(3)}(\omega, I). \quad (20)$$

The linear and third-order nonlinear parts of the AC are respectively:

$$\alpha^{(1)}(\omega) = \omega\sqrt{\frac{\mu_1}{\varepsilon}}\frac{\sigma_1 \hbar\Gamma_{fi}|M_{fi}|^2}{(E_{fi} - \hbar\omega)^2 + (\hbar\Gamma_{fi})^2}, \quad (21)$$

$$\alpha^{(3)}(\omega, I) = -\omega\sqrt{\frac{\mu_1}{\varepsilon}}\left(\frac{I}{2\varepsilon_0 n_r c}\right)\frac{4\sigma_1 \hbar\Gamma_{fi}|M_{fi}|^4}{\left[(E_{fi} - \hbar\omega)^2 + (\hbar\Gamma_{fi})^2\right]^2} \times \left[1 - \frac{|M_{ff} - M_{ii}|^2}{4|M_{fi}|^2}\frac{3E_{fi}^2 - 4\hbar\omega E_{fi} + \hbar^2(\omega^2 - \Gamma_{fi}^2)}{E_{fi}^2 + (\hbar\Gamma_{fi})^2}\right]. \quad (22)$$

3 Results and discussions

We investigate the effects of hydrostatic pressure, temperature and QD size on the optical properties including the linear, third-order nonlinear of the ACs and RIs related to the $1s-1p$ transition of exciton in a spherical GaAs QD. The physical parameters used in our calculation are given in Table 1.

In the beginning, we should notice that the energies difference $E_{\rm fi}=E_{1p}-E_{1s}$ and the dipole matrix element $|M_{\rm fi}|$ are the principal parameters influencing the oscillator strength, and consequently modify the linear and nonlinear optical properties. In Fig. 1, we present the first energy transition $E_{\rm fi}=E_{1p}-E_{1s}$ for $(P=0,\ T=0\,\text{K})$, $(P=20\,\text{kbar},\ T=0\,\text{K})$ and $(P=0,\ T=300\,\text{K})$ as a function of QD sizes. It appears that under the effect of the hydrostatic pressure, the shift between the fundamental and the first excited states increases, whereas the temperature tends to reduce this energy difference. Due to the fact that, in strong confinement, the kinetic energy of the uncorrelated electron and hole dominates the total energy of exciton, the magnitude of $1s-1p$ transition is more pronounced for small sizes. The same behavior is observed in GaAs/$Ga_{0.7}Al_{0.3}As$ QD described by a quasi 3D classical parabolic potential and using a perturbative approach [21]. We are limiting the pressure value to 20 kbar because when the outer matrix of the dot is for example GaAlAs, the hydrostatic pressure induces a crossover between the Γ and *X* conduction bands. In this case, near to 30 kbar the system turns in a metallic structure and there is not confinement effect on the carriers.

In Fig. 2, we plot the variation of the dipole matrix element $|M_{\rm fi}|$ as a function of QD sizes under the pressure and temperature effects. As it can be seen, $|M_{\rm fi}|$ increases with increasing dot size. The pressure and temperature have opposite effects on the $|M_{\rm fi}|$ behavior. Indeed, the pressure reduces the intensity of $|M_{\rm fi}|$ while the augmentation of the temperature reinforces it. We note that the temperature and pressure effects are very sensitive to the QD size. The influence of *P* and *T* are less pronounced for smaller sizes than for larger ones. Our calculations are in good agreement with the conclusions existing in the studies related to the donor impurities [38, 39].

Figures 3 and 4 present the behaviors of different parts of the ACs and RIs. In Fig. 3, we draw the linear, third

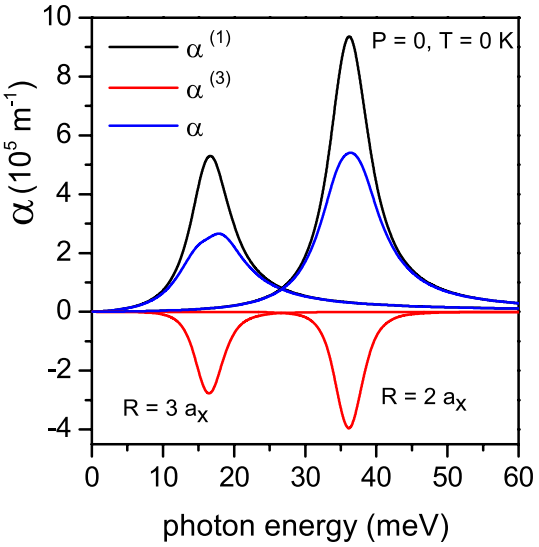

Fig. 3 The linear, third nonlinear and total absorption coefficients as functions of incident photon energy for $R=2$ and $3a_X$

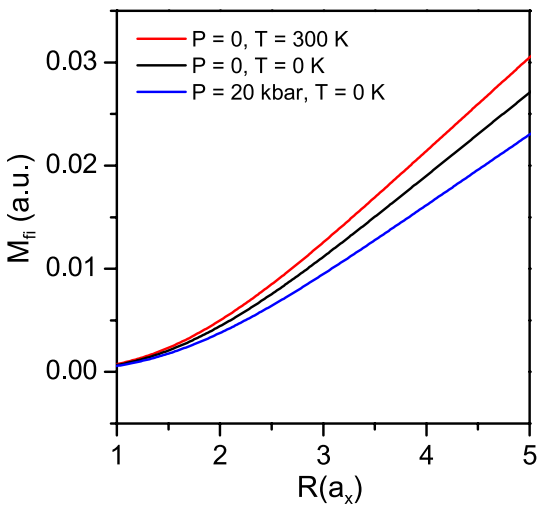

Fig. 2 The electric dipole transition matrix element of an exciton as a function of the dot radius for $(P=0,\ T=0\ \text{K})$, $(P=0,\ T=300\ \text{K})$ and $(P=20\ \text{kbar},\ T=0\ \text{K})$

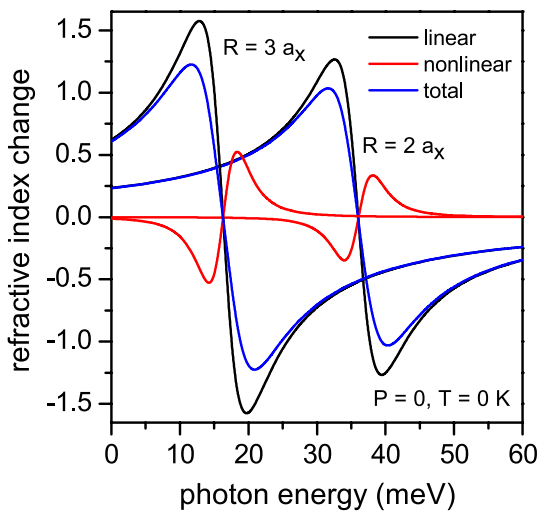

Fig. 4 The linear, third nonlinear and total refractive index changes versus the incident photon energy for $R=2$ and $3a_X$

nonlinear and total ACs as functions of the incident photon energy without taking into account the pressure and temperature effects for two size values corresponding to $R = 2\,a_X$ and $3\,a_X$. First of all, we notice that the linear AC constitute the principal contribution in the total AC. The nonlinear AC has also a not negligible contribution but it varies oppositely with the linear AC, so the addition of the nonlinear term reduces the total AC.

On the other hand, we can clearly see that all components of ACs are deeply influenced by the variation of the dot sizes. It is known that the energy of the exciton decreases when the radius increases, due to the spreading of the electronic density. This leads to a weakness of the Coulomb interaction effect and the electron and hole are moving away from each other. Thus the system relaxes and the transition $E_{\mathrm{fi}} = E_{1p} - E_{1s}$ becomes less important as discussed before in Fig. 1. As consequence, the peaks of the ACs exhibit a red shift (blue shift) when the dot size increases (decreases). The amplitude of the peaks increases for strong confinement because the strength of AC is dominated by the value of the energy difference E_{fi}. In Fig. 4, the RIs are plotted as functions of the incident photon energy, we find that the RIs follow the same behavior as the ACs, and shift toward the lower energies (red shift), when the QD size becomes larger.

In order to understand the pressure effects, we present in Fig. 5 and 6 the linear and third nonlinear components of the total AC and of the RI, respectively, as functions of the photon energy $\hbar\omega$, for three significant values of pressure ($P = 0$, $P = 10$ and $P = 20$ kbar) and for two QD sizes ($R = 2\,a_X$ and $R = 3\,a_X$).

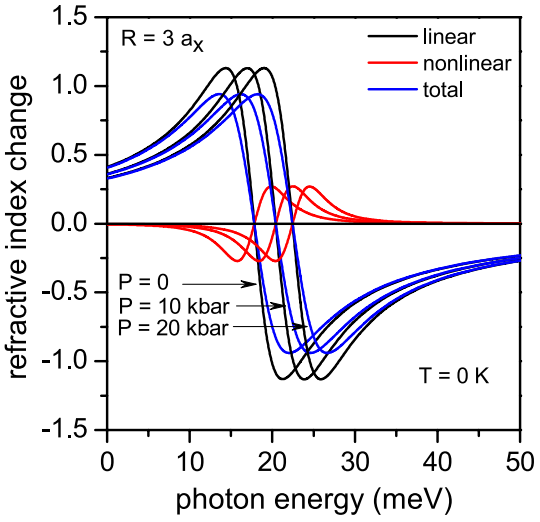

Fig. 6 The linear, third nonlinear and total refractive index changes versus the incident photon energy for $R = 3a_X$ and 3 values of pressure: $P = 0$, 10 and 20 kbar

As expected, in Fig. 5, we observe that by increasing the pressure, the ACs peaks are shifted to high energy region and their intensities are reinforced. This due to the fact that the pressure effect reinforces the spatial confinement by shrinking the orbital wave functions and acts as a additive confinement and consequently a strengthening of the optical properties can be observed. Our conclusions are in good agreement with different previous works concerning the donor systems [40, 41]. Note that our results disagree with those of Lu et al. [21] where their model predicts a

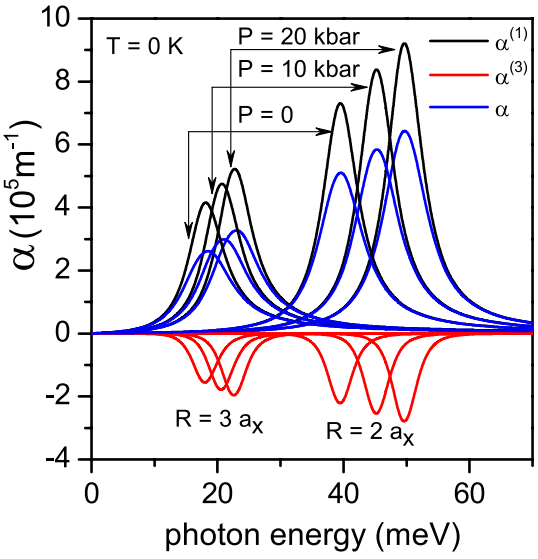

Fig. 5 The linear, third nonlinear and total absorption coefficients as functions of incident photon energy for 3 values of pressure: $P = 0$, 10 and 20 kbar, for $R = 2$ and $3a_X$

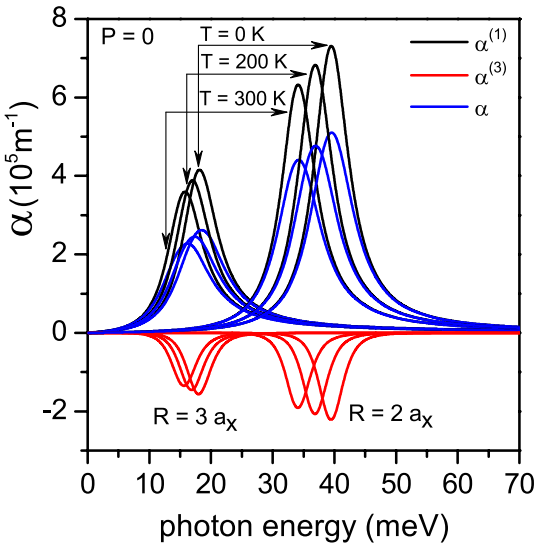

Fig. 7 The linear, third nonlinear and total absorption coefficients as functions of the incident photon energy for 3 values of temperature: $T = 0$, 200 and 300 K, for $R = 2$ and $3a_X$

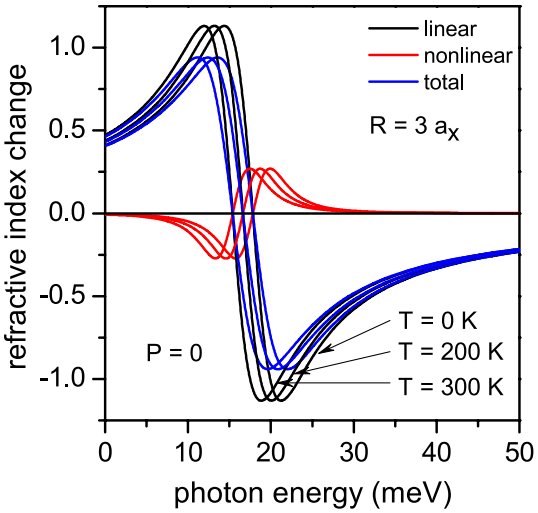

Fig. 8 The linear, third nonlinear and total refractive index changes versus the incident photon energy for $R = 3a_X$ and 3 values of temperature: $T = 0$, 200 and 300 K

decrease of intensity for the high pressures. By analyzing the AC and RI variations (Fig. 6), different aspects can be detected: a significant increase in AC and a small decrease for RI. These different evolutions can be explained by means of the expressions of AC and RI. Equations (21) and (22) show that AC is related to the electric dipole matrix element, the transition energy E_{fi} and the dielectric constant $\varepsilon(P)$. These quantities do not depend on the pressure in the same way, which leads to a competition between these three terms. Our numerical calculations show that the introduction of the pressure induces a small change in $|M_{\text{fi}}|$ and E_{fi} compared to $\varepsilon(P)$, so the AC magnitude is dominated by the value of the pressure-dependent dielectric constant. On the other hand, contrarily to what happens for AC, the Eqs. (18) and (19) show that RI is independent of ε what explains the slight increase of RI with increasing pressure.

To know how the temperature influences the ACs and RIs, we plot in Fig. 7 the variations of ACs as functions of the photon energy, for three different values of temperature ($T = 0$ K, $T = 200$ K and $T = 300$ K) and for two QD radii ($R = 2\,a_X$ and $R = 3\,a_X$). Our results show that, as the temperature increases, the ACs peaks move to the lower energies for all confinement regimes. This red shift is accompanied with a diminution of the peak intensities of both AC. This is due to the decreasing in the energy transition between the initial and final states as function of temperature as mentioned in Fig. 1. Indeed, the variations of the electron and hole effective masses and of the band gap energy of GaAs as functions of the temperature lead to a decreasing of the uncorrelated electron hole energies in the confined systems. In Fig. 8, the RIs are plotted as functions of the photon energy, for three different values of temperature $T = 0$ K, $T = 200$ K and $T = 300$ K for $R = 3\,a_X$. As we can see, the RIs strongly depend on the temperature and their peaks move toward the lower energies contrary to the results obtained by Lu et al. [21] who used a perturbation method with a parabolic potential to model the confinement.

4 Conclusion

In the present work, we have determined the nonlinear optical properties of an exciton confined in a GaAs spherical quantum dot under the effects of hydrostatic pressure and temperature using the variational method by taking into account the QD sizes. Our results show that the optical properties of QDs strongly depend on the QD size, hydrostatic pressure and temperature. By increasing the pressure, the ACs and RIs curves shift toward the higher energies (blue shift) but increasing temperature and QD sizes induce a displacement of the optical responses (AC and RI) to lower energies (red shift). We underline the simplicity and robustness of our model taking into account the Coulomb interaction between the electron and hole and using the Hylleraas coordinates and we hope that it can contribute to a better understanding of the optical properties associated to transitions specific to excitonic states $1s - 1p$ towards low powers optoelectronic devices such as modulators, optical switches or injection lasers.

Acknowledgements C. A. Duque acknowledges the support by Colombian Agencies: CODI-Universidad de Antioquia (Estrategia de Sostenibilidad de la Universidad de Antioquia and projects "Efectos de capas delta dopadas en pozos cuánticos como fotodetectores en el infrarrojo" and "Efectos ópticos intersubbanda, no lineales de segundo orden y dispersión Raman, en sistemas asimétricos de pozos cuánticos acoplados"), and Facultad de Ciencias Exactas y Naturales-Universidad de Antioquia (CAD-exclusive dedication project 2018–2019). This work used resources of the Centro Nacional de Processamento de Alto Desempenho em São Paulo (CENAPAD-SP).

References

1. T. Jamieson, R. Bakhshi, D. Petrova, R. Pocock, M. Imani, A.M. Seifalian, Biomaterials **28**, 4717–4732 (2007)
2. O. Salata, J. Nanobiotechnol. **2**, 1–6 (2004)
3. D. Mocatta, G. Cohen, J. Schattner, O. Millo, E. Rabani, U. Banin, Science **332**, 77–81 (2011)
4. P.M. Koenraad, M.E. Flatté, Nat. Mater. **10**, 91–100 (2011)
5. P. Harrison, *Quantum wells, wires and dots* (Wiley, New York, 2006)
6. G. Schmid, *Nanoparticles from theory to applications*, second edn. (Wiley-VCH, Velag GmbH & Co KGaA, New York, 2010)
7. I. Karabulut, S. Baskoutas, J. Appl. Phys. **103**, 073512 (2008)
8. H.M. Baghramyan, M.G. Barseghyan, A.A. Kirakosyan, R.L. Restrepo, C.A. Duque, J. Lumin. **134**, 594–599 (2013)

9. J.C. Martinez-Orozco, K.A. Rodriguez-Magdaleno, J.R. Suarez-Lopez, C.A. Duque, R.L. Restrepo, Superlattices Microstruct. **92**, 166–173 (2016)
10. I. Karabulut, M.E. Mora-Ramos, C.A. Duque, J. Lumin. **131**, 1502–1509 (2011)
11. H. Yildirim, M. Tomak, Eur. Phys. J. B **50**, 559–564 (2006)
12. R. Kostić, D. Stojanović, J. Nanophotonics **5**, 051810 (2011)
13. S. Baskoutas, A.F. Terzis, Eur. Phys. J. B **69**, 237–244 (2009)
14. W. Xie, Phys. B **405**, 3436–3440 (2010)
15. E.C. Niculescu, M. Cristea, J. Lumin. **135**, 120–127 (2013)
16. M. El Haouari, A. Talbi, E. Feddi, H. El Ghazi, A. Oukerroum, F. Dujardin, Opt. Commun. **383**, 231–237 (2017)
17. I. Mal, J. Jayarubi, S. Das, A.S. Sharma, A.J. Peter, D.P. Samajdar, Phys. Status Solidi B (2018). https://doi.org/10.1002/pssb.201800395
18. E. Owji, A. Keshavarz, H. Mokhtari, Superlattices Microstruct. **98**, 276–282 (2016)
19. E. Aksahin, V. Ustoglu Unal, M. Tomak, Phys. E **74**, 258–263 (2015)
20. E. Hanamura, Phys. Rev. B **37**, 1273–1279 (1988)
21. L. Lu, W. Xie, Z. Shu, Phys. B **406**, 3735–3740 (2011)
22. Z. Zeng, G. Gorgolis, C.S. Garoufalis, S. Baskoutas, Sci. Adv. Mater. **6**, 1–6 (2014)
23. S.Y. Lopez, N. Porras-Montenegro, C.A. Duque, Phys. Status Solidi (b) **246**, 630–634 (2009)
24. C.A. Duque, S.Y. Lopez, M.E. Mora-Ramos, Phys. Status Solidi (b) **244**, 1964–1970 (2007)
25. P.Y. Yu, M. Cordona, *Fundamentals of semiconductors* (Springer, Berlin, 1998)
26. F.J. Culchac, N. Porras-Montenegro, A. Latge, J. Appl. Phys. **105**, 094324 (2009)
27. H.M. Baghramyan, M.G. Barseghyan, A.A. Kirakosyan, R.L. Restrepo, C.A. Duque, J. Lumin. **134**, 594–599 (2013)
28. M.G. Barseghyan, M.E. Mora-Ramos, C.A. Duque, Eur. Phys. J. B **84**, 265–271 (2011)
29. F. Dujardin, E. Feddi, A. Oukerroum, J. Bosch Bailach, J. Martinez-Pastor, E. Assaid, J. Appl. Phys. **113**, 064314 (2013)
30. E. Feddi, A. Zouitine, A. Oukerroum, F. Dujardin, E. Assaid, M. Zazoui, J. Appl. Phys. **117**, 064309 (2015)
31. F. Dujardin, E. Feddi, E. Assaid, A. Oukerroum, Eur. Phys. J. B **74**, 507–516 (2010)
32. J.V. Atanasoff, Phys. Rev. **36**, 1232–1242 (1930)
33. M. Abramowitz, I.A. Stegun (eds.), *Handbook of mathematical functions* (Dover, New York, 1972)
34. M.R.K. Vahdani, G. Rezaei, Phys. Lett. A **373**, 3079–3084 (2009)
35. A.R. Jafari, Phys. B **456**, 72–77 (2015)
36. J. Abraham, Hudson Mark, A. John Peter, J. Semicond. **33**, 092001 (2012)
37. A.John Peter, Phys. E **28**, 225–229 (2005)
38. H. El Ghazi, A. Jorio, I. Zorkani, Opt. Commun. **331**, 73–76 (2014)
39. S.J. Liang, W.F. Xie, Eur. Phys. J. B **80**, 79–84 (2011)
40. R. Khordad, Phys. B **407**, 1128–1133 (2012)
41. G. Staszczak, I. Gorczyca, T. Suski, X.Q. Wang, N.E. Christensen, A. Svane, E. Dimakis, T.D. Moustakas, J. Appl. Phys. **113**, 123101 (2013)